Composite Structures 118 (2014) 560–570

Contents lists available at ScienceDirect

Composite Structures

journal homepage: www.elsevier.com/locate/compstruct

Implementation of the refined zigzag theory in shell elements with large displacements and rotations

Fernando G. Flores *

Departamento de Estructuras, Universidad Nacional de Córdoba and CONICET, Casilla de Correo 916, 5000 Córdoba, Argentina

ARTICLE INFO

Article history:
Available online 13 August 2014

Keywords:
Finite elements
Shells
Refined zigzag
Sandwich laminate

ABSTRACT

This work shows a possible implementation of the refined zigzag theory in elements based on Simo's shell theory. Refined zigzag theory can deal with composite laminate economically, adding only two nodal degrees of freedom, with very good accuracy. Two existing elements are considered, a four-node bi-linear quadrilateral and a six-node linear triangle. This geometry is enhanced with a hierarchical field of in-plane displacement expressed in convective coordinates. The objective is to have simple and efficient elements to analyze composite laminates under large displacements and rotations but small elastic strains. General aspects of the implementation are presented, and in particular the assumed natural strain technique used to prevent transverse shear locking. Several examples are considered to compare on the one hand with analytical static solutions and natural frequencies of plates, and on the other hand to observe the buckling loads and non-linear behavior with large displacement in double curved shells. In these latter cases comparisons are against numerical solutions obtained with solid elements. The results obtained are in a very good agreement with the targets used.

1. Introduction

Both the classical theory of thin shells [7] and the first order transverse shear deformation theory (FSDT, [12]) lead to good results in treating homogeneous materials. However, the basic hypothesis that assumes that fibers in the direction normal to the shell will remain straight leads to poor predictions when dealing with materials with a high degree of heterogeneity across the thickness.

In order to improve predictions, theories with higher order (cubic or higher) interpolation of displacements in the thickness of the shell have been proposed (see for example the monograph [10]) but their use is not widespread because their predictive power is unreliable.

A three-dimensional analysis using solid elements appears as the most suitable technique for the treatment of composite materials, but it can easily become prohibitively expensive due to the number of layers in the laminate that may be greater than 100. In such cases multiple layers may be grouped together within one single layer with combined properties in order to maintain the number of degrees of freedom (DoFs) of the problem within manageable limits [8].

More precise techniques than those based on shell theories are layer-wise approaches, in which the thickness of the laminate is divided into a number of layers (which may or may not coincide with the physical number of layers) assuming a linear variation of displacements (in the plane of the layer) between layers. A review of these techniques can be seen in [11]. This approach clearly suffers from the same problem of using three-dimensional solid elements for the analysis.

The analysis made with solid element models and layer-wise approaches show that the profile of the in-plane displacement along the normal to the plane of the laminate can not be approximated by a polynomial of higher order. That has led to the appearance of zigzag approximations where the interpolation functions are only C^0 continuous across the thickness and with a zigzag profile, i.e. the first derivative (with associated transverse shear deformation) is discontinuous. This naturally occurs due to the different modules of transverse elasticity of each layer, which may differ by several orders of magnitude. In [1] a review of these theories may be seen. Recently a refined version of this proposal [15] has been presented, that based on the FSDT (5 DoFs), two additional DoFs are included, representing the amplitudes of hierarchical in-plane

* Address: Departamento de Estructuras, Universidad Nacional de Córdoba and CONICET, Casilla de Correo 916, 5000 Córdoba, Argentina. Tel.: +54 351 5353800x721.
E-mail address: fflores@efn.uncor.edu

http://dx.doi.org/10.1016/j.compstruct.2014.07.034
0263-8223/

displacements added to the linear through-the-thickness assumption kinematics. This theory involves constant transverse shear stresses in each layer (and therefore discontinuous) but allows treating clamped boundary conditions that is a limitation present in early zigzag theories.

These refined zigzag theories (ZZRT) have been implemented in 2D beam elements [5,9] and flat plate elements [15,2,6] where a very good approximation has been reported for the displacement field across the laminate thickness. It was also reported that the shear stresses directly obtained using the constitutive relation and the shear deformations computed from the displacement field show a poor approximation. An accurate recovery of transverse shear stresses requires integration across the laminate thickness of the equilibrium equations in the plane of the sheet, for which the derivatives of the stresses between finite elements must be evaluated.

In the author's knowledge the ZZRT has not been used in double curvature shells. Furthermore geometrically nonlinear models for plates resort to the use of von Kármán plate kinematics in order to evaluate buckling loads.

In this paper a possible implementation of the ZZRT on shell elements based on the geometrically exact shell theory of Simo [13] is presented. The elements considered are a bi-linear 4-node quadrilateral and a linear 6-node triangle, the latter with a no-conforming interpolation of the field director [4]. The scope of this work is restricted to small elastic strains but large displacements and rotations.

An outline of this paper is as follows. The basic kinematic of the base shell theory by Simo (FSDT) is summarized in the next section. Then additional displacement fields (ZZRT) are introduced and a possible way to obtain the across the thickness interpolation is explained. Resulting elasticity matrices for the new generalized stress and strain measures are then evaluated. Section 6 summarizes the base shell elements used and the modifications required to include the ZZRT approximation while in Section 7 the transverse shear approach to avoid locking is explained. Several examples are presented in Section 8 to compare linear plate models with theoretical results and non-linear shell models with 3D solid discretizations. Finally some conclusions are summarized.

2. Basic kinematics

For a formulation in large displacements and rotations and small strains compatible with an elastic composite laminate, we start from the approach proposed by Simo et al. [13] where the configuration of the shell is defined by the position of the middle surface $\boldsymbol{\varphi}$ and the field director $\mathbf{t}$ (pseudo normal). The positions of a material point before and after the deformation are written as

$$\mathbf{X}(x,y,z) = \boldsymbol{\varphi}_0(x,y) + z\mathbf{t}_0(x,y) \tag{1}$$

$$\mathbf{x}(x,y,z) = \boldsymbol{\varphi}(x,y) + z\mathbf{t}(x,y) \tag{2}$$

$$\boldsymbol{\Lambda}(x,y) = [\,\mathbf{t}_1 \quad \mathbf{t}_2 \quad \mathbf{t}_3\,] \tag{3}$$

where (x,y,z) are convective coordinates in a suitably chosen local system with z in the direction of the director and (x,y) are associated with two orthogonal directions in the tangent plane to the middle surface. The director $\mathbf{t}$ is the third component ($\mathbf{t}_3$) of the local triad $\boldsymbol{\Lambda}$ and it is assumed that for small strains the thickness does not change during the deformation.

The relevant strain measures are obtained first evaluating the deformation gradient relative to the convective system

$$\mathbf{F} = \frac{\partial \mathbf{x}}{\partial \mathbf{X}} = \left[\boldsymbol{\varphi}_x + z\mathbf{t}_x, \boldsymbol{\varphi}_y + z\mathbf{t}_y, \mathbf{t}\right] \tag{4}$$

and with it the right Cauchy–Green tensor results

$$\mathbf{C} = \mathbf{F}^T\mathbf{F} = \begin{bmatrix} \boldsymbol{\varphi}_x\cdot\boldsymbol{\varphi}_x & \boldsymbol{\varphi}_x\cdot\boldsymbol{\varphi}_y & \boldsymbol{\varphi}_x\cdot\mathbf{t} \\ \boldsymbol{\varphi}_y\cdot\boldsymbol{\varphi}_x & \boldsymbol{\varphi}_y\cdot\boldsymbol{\varphi}_y & \boldsymbol{\varphi}_y\cdot\mathbf{t} \\ \mathbf{t}\cdot\boldsymbol{\varphi}_x & \mathbf{t}\cdot\boldsymbol{\varphi}_y & 1 \end{bmatrix} + z\begin{bmatrix} \mathbf{t}_x\cdot\boldsymbol{\varphi}_x & \mathbf{t}_x\cdot\boldsymbol{\varphi}_y & 0 \\ \mathbf{t}_y\cdot\boldsymbol{\varphi}_x & \mathbf{t}_y\cdot\boldsymbol{\varphi}_y & 0 \\ 0 & 0 & 0 \end{bmatrix} + z^2\begin{bmatrix} \mathbf{t}_x\cdot\mathbf{t}_x & \mathbf{t}_x\cdot\mathbf{t}_y & 0 \\ \mathbf{t}_y\cdot\mathbf{t}_x & \mathbf{t}_y\cdot\mathbf{t}_y & 0 \\ 0 & 0 & 0 \end{bmatrix} \tag{5}$$

where the terms associated with z^2 are commonly neglected. Then it can be distinguished

- The metric tensor of the middle surface

$$\begin{bmatrix} a_{xx} \\ a_{yy} \\ 2a_{xy} \end{bmatrix} = \begin{bmatrix} \boldsymbol{\varphi}_x\cdot\boldsymbol{\varphi}_x \\ \boldsymbol{\varphi}_y\cdot\boldsymbol{\varphi}_y \\ 2\boldsymbol{\varphi}_x\cdot\boldsymbol{\varphi}_y \end{bmatrix} \tag{6}$$

and the Green Lagrange strain tensor of the middle surface

$$\begin{bmatrix} E_{xx} \\ E_{yy} \\ 2E_{xy} \end{bmatrix} = \frac{1}{2}\begin{bmatrix} a_{xx}-1 \\ a_{yy}-1 \\ 2a_{xy} \end{bmatrix} = \mathbf{E}_m \tag{7}$$

- the pseudo curvature tensor

$$\begin{bmatrix} \kappa_{xx} \\ \kappa_{yy} \\ 2\kappa_{xy} \end{bmatrix} = \frac{1}{2}\begin{bmatrix} \mathbf{t}_x\cdot\boldsymbol{\varphi}_x \\ \mathbf{t}_y\cdot\boldsymbol{\varphi}_y \\ \mathbf{t}_x\cdot\boldsymbol{\varphi}_y + \mathbf{t}_y\cdot\boldsymbol{\varphi}_x \end{bmatrix} \tag{8}$$

that allows to compute curvature changes from the original configuration

$$\begin{bmatrix} \chi_{xx} \\ \chi_{yy} \\ 2\chi_{xy} \end{bmatrix} = \begin{bmatrix} \kappa_{xx} \\ \kappa_{yy} \\ 2\kappa_{xy} \end{bmatrix} - \begin{bmatrix} \kappa^0_{xx} \\ \kappa^0_{yy} \\ 2\kappa^0_{xy} \end{bmatrix} = \boldsymbol{\chi} \tag{9}$$

- the transverse shear strains

$$\begin{bmatrix} a_{zx} \\ a_{zy} \end{bmatrix} = \begin{bmatrix} \mathbf{t}\cdot\boldsymbol{\varphi}_x \\ \mathbf{t}\cdot\boldsymbol{\varphi}_y \end{bmatrix} \tag{10}$$

$$\begin{bmatrix} \gamma_{xz} \\ \gamma_{yz} \end{bmatrix} = \begin{bmatrix} \mathbf{t}\cdot\boldsymbol{\varphi}_x - \mathbf{t}^0\cdot\boldsymbol{\varphi}^0_x \\ \mathbf{t}\cdot\boldsymbol{\varphi}_y - \mathbf{t}^0\cdot\boldsymbol{\varphi}^0_y \end{bmatrix} = \begin{bmatrix} a_{zx} \\ a_{zy} \end{bmatrix} - \begin{bmatrix} a^0_{zx} \\ a^0_{zy} \end{bmatrix} \tag{11}$$

These generalized strains allow to obtain the strain tensor at any point across the thickness.

3. Additional displacement field

To consider the use of the ZZRT it is necessary to distinguish displacements in the direction of the director and displacements in the tangent plane to the middle surface. Besides, these new displacements are additional to the basic kinematics (i.e. hierarchical DoFs). The zigzag functions are introduced into the convective local coordinate system with components in the tangent plane of the shell (directions (x,y))

$$\begin{bmatrix} u(x,y,z) \\ v(x,y,z) \end{bmatrix} = \begin{bmatrix} \phi_x(z) & \\ & \phi_y(z) \end{bmatrix}\begin{bmatrix} \psi_x(x,y) \\ \psi_y(x,y) \end{bmatrix} \tag{12}$$

$$\mathbf{u}(x,y,z) = \boldsymbol{\phi}(z)\boldsymbol{\psi}(x,y)$$

where $\boldsymbol{\psi}$ is the amplitude of the hierarchical displacement and the hierarchical interpolation function across the thickness $\phi_i(z)$ (zigzag function) is null at both bottom and top shell surfaces

$$\boldsymbol{\phi}\left(\pm\frac{h}{2}\right) = \mathbf{0} \tag{13}$$

while its derivative with respect to the transverse coordinate (z), assumed constant within each layer,

$$\beta_i^k = \frac{\phi_i^k - \phi_i^{k-1}}{z^k - z^{k-1}} = \frac{\phi_i^k - \phi_i^{k-1}}{h^k} \tag{14}$$

$$\sum \beta_i^k h^k = 0 \tag{15}$$

depends solely on the properties of the laminate.

As the scope of this work is restricted to small strains, the results of the ZZRT [15] can directly be used to enhance the in-plane strain components at each layer k of the laminate in the form:

$$\mathbf{E}_m^k = \mathbf{E}_m + z^k \boldsymbol{\chi} + \boldsymbol{\Phi}^k \nabla\psi \tag{16}$$

where two matrices have been defined that include the hierarchical shape functions $\boldsymbol{\phi}$ and the in-plane gradient of the amplitudes

$$\boldsymbol{\phi}^k = \begin{bmatrix} \phi_x^k & & \\ & \phi_y^k & \\ & & \phi_x^k \quad \phi_y^k \end{bmatrix} \qquad \nabla\boldsymbol{\psi} = \begin{bmatrix} \psi_{x'x} \\ \psi_{y'y} \\ \psi_{x'y} \\ \psi_{y'x} \end{bmatrix} \tag{17}$$

While the transverse shear strain is now the sum

$$\begin{bmatrix} \gamma_{xz}^k \\ \gamma_{yz}^k \end{bmatrix} = \begin{bmatrix} \gamma_{xz} \\ \gamma_{yz} \end{bmatrix} + \begin{bmatrix} \beta_x^k \psi_x \\ \beta_y^k \psi_y \end{bmatrix} = \left[\mathbf{1}_2, \boldsymbol{\beta}^k\right] \begin{bmatrix} \boldsymbol{\gamma} \\ \boldsymbol{\psi} \end{bmatrix}$$
$$\boldsymbol{\gamma}^k = \mathbf{S}_t^k \boldsymbol{\varepsilon}_t \tag{18}$$

where $\mathbf{1}_2$ is the identity matrix of order 2 and we have defined the diagonal matrix

$$\boldsymbol{\beta}^k = \begin{bmatrix} \beta_x^k & \\ & \beta_y^k \end{bmatrix} \tag{19}$$

4. Determination of the zigzag functions

The ZZRT [15] indicates a way to obtain zigzag functions $\boldsymbol{\phi}$. Note first that by the properties of the functions $\boldsymbol{\phi}$ (Eq. (13))

$$\int_h \gamma_{iz}(z)dz = \int_h (\gamma_{iz} + \beta_i\psi_i)dz = \gamma_{iz}h \tag{20}$$

The stresses in each layer, separating in-plane components and transverse shear components, are

$$\boldsymbol{\sigma}^k = \begin{bmatrix} \sigma_{xx}^k \\ \sigma_{yy}^k \\ \tau_{xy}^k \end{bmatrix} = \mathbf{D}_p^k \mathbf{E}^k = \mathbf{D}_p^k \mathbf{S}_p^k \boldsymbol{\varepsilon}_p \tag{21}$$

$$\boldsymbol{\tau}^k = \begin{bmatrix} \tau_{xz}^k \\ \tau_{yz}^k \end{bmatrix} = \mathbf{D}_t^k \boldsymbol{\gamma}^k = \mathbf{D}_t^k \mathbf{S}_t^k \boldsymbol{\varepsilon}_t \tag{22}$$

where the in-plane and transverse elasticity matrices of each layer $\mathbf{D}_p^k$ and $\mathbf{D}_t^k$ are in general full matrices. In particular the transverse strain components can be written from Eq. (18) as

$$\gamma_{iz}^k = \gamma_i + \beta_i^k \psi_i = (\gamma_i - \psi_i) + \left(1 + \beta_i^k\right)\psi_i = \eta_i + \left(1 + \beta_i^k\right)\psi_i \tag{23}$$

Replacing in the transverse shear stresses (22) and regrouping

$$\begin{bmatrix} \tau_{xz}^k \\ \tau_{yz}^k \end{bmatrix} = \begin{bmatrix} G_{xx}^k & G_{xy}^k \\ G_{xy}^k & G_{yy}^k \end{bmatrix} \begin{bmatrix} \eta_x + \left(1 + \beta_x^k\right)\psi_x \\ \eta_y + \left(1 + \beta_y^k\right)\psi_y \end{bmatrix}$$
$$= \begin{bmatrix} G_{xx}^k & G_{xy}^k \\ G_{xy}^k & G_{yy}^k \end{bmatrix} \begin{bmatrix} \eta_x \\ \eta_y \end{bmatrix} + \begin{bmatrix} G_{xx}^k\left(1 + \beta_x^k\right) & G_{xy}^k\left(1 + \beta_y^k\right) \\ G_{xy}^k\left(1 + \beta_x^k\right) & G_{yy}^k\left(1 + \beta_y^k\right) \end{bmatrix} \begin{bmatrix} \psi_x \\ \psi_y \end{bmatrix} \tag{24}$$

If the diagonal term which multiplies each ψ_j is made constant through the thickness

$$G_{ii}^k\left(1 + \beta_i^k\right) = G_i = \text{cte.} \tag{25}$$

allows to obtain a possible distribution of the β_i^k across the thickness

$$\beta_i^k = \frac{G_i}{G_{ii}^k} - 1 \tag{26}$$

while the condition

$$\int_h \beta_i dh = \sum_{k=1}^N \beta_i^k h^k = \sum_{k=1}^N \left(\frac{G_i}{G_{ii}^k} - 1\right) h^k = G_i \sum_{k=1}^N \frac{h^k}{G_{ii}^k} - \sum_{k=1}^N h^k = 0 \tag{27}$$

allows to obtain each G_i in the form

$$G_i = \frac{\int_h dh}{\int \frac{dh}{G_{ii}^k}} = \frac{h}{\sum_{k=1}^N \frac{h_k}{G_{ii}^k}} \tag{28}$$

then

$$G_{xy}^k\left(1 + \beta_x^k\right) = G_{xy}^k\left(\frac{G_x}{G_{xx}^k}\right) = G_x\left(\frac{G_{xy}^k}{G_{xx}^k}\right) \tag{29}$$

$$G_{yx}^k\left(1 + \beta_y^k\right) = G_{yx}^k\left(\frac{G_y}{G_{yy}^k}\right) = G_y\left(\frac{G_{yx}^k}{G_{yy}^k}\right) \tag{30}$$

This gives a possible way to obtain the derivatives of the zigzag functions across the laminate thickness. The variable $\boldsymbol{\eta}$ is not use below, the shear stress are computed using (22) and the shear forces are obtained integrating across the thickness.

5. Equivalent elasticity matrices and stress measures

Associated with the hierarchical strains new stress measures appear. For a linear elastic material the internal strain energy per unit of middle surface is:

$$\begin{aligned} W &= \frac{1}{2}\int_h \left(\mathbf{E}^k \cdot \boldsymbol{\sigma}^k + \boldsymbol{\gamma}^k \cdot \boldsymbol{\tau}^k\right) dz \\ &= \frac{1}{2}\int_h \left(\boldsymbol{\varepsilon}_p^T \mathbf{S}_p^T \mathbf{D}_p^k \mathbf{S}_p \boldsymbol{\varepsilon}_p + \boldsymbol{\varepsilon}_t^T \mathbf{S}_t^T \mathbf{D}_t^k \mathbf{S}_t \boldsymbol{\varepsilon}_t\right) dz \\ &= \frac{1}{2}\int_h \left(\boldsymbol{\varepsilon}_p^T \begin{bmatrix} \mathbf{1}_3 \\ z\mathbf{1}_3 \\ \boldsymbol{\Phi}^k \end{bmatrix} \mathbf{D}_p^k \left[\mathbf{1}_3, z\mathbf{1}_3, \boldsymbol{\Phi}^k\right] \boldsymbol{\varepsilon}_p + \boldsymbol{\varepsilon}_t^T \begin{bmatrix} \mathbf{1}_2 \\ \boldsymbol{\beta}^k \end{bmatrix} \mathbf{D}_t^k \left[\mathbf{1}_2, \boldsymbol{\beta}^k\right] \boldsymbol{\varepsilon}_t\right) dz \end{aligned} \tag{31}$$

where energy is written as a quadratic form of the generalized strains defined in (16) and (18) in order to obtain the conjugated generalized stresses. Defining for the shell in-plane components

$$(\mathbf{D}_p)_{10\times 10} = \int_h \begin{bmatrix} \mathbf{1}_3 \\ -z\mathbf{1}_3 \\ \boldsymbol{\Phi}^k \end{bmatrix}_{10\times 3} \left(\mathbf{D}_p^k\right)_{3\times 3} \left[\mathbf{1}_3, z\mathbf{1}_3, \boldsymbol{\Phi}^k\right]_{3\times 10} dz$$
$$= \begin{bmatrix} \left(\mathbf{D}_p^{11}\right)_{3\times 3} & \left(\mathbf{D}_p^{12}\right)_{3\times 3} & \left(\mathbf{D}_p^{13}\right)_{3\times 4} \\ & \left(\mathbf{D}_p^{22}\right)_{3\times 3} & \left(\mathbf{D}_p^{23}\right)_{3\times 4} \\ \text{sim} & & \left(\mathbf{D}_p^{33}\right)_{4\times 4} \end{bmatrix} \tag{32}$$

where $\mathbf{D}_p^{11}$, $\mathbf{D}_p^{12}$ and $\mathbf{D}_p^{22}$ are the standard terms that appear when dealing with laminates for thin shell theories. While for the transverse shear components

$$(\mathbf{D}_t)_{4\times4} = \int_h \begin{bmatrix} \mathbf{1}_2 \\ \boldsymbol{\beta}^k \end{bmatrix}_{4\times2} \left(\mathbf{D}_t^k\right)_{2\times2} \left[\mathbf{1}_2, \boldsymbol{\beta}^k\right]_{2\times4} dz = \int_h \begin{bmatrix} \mathbf{D}_t^k & \mathbf{D}_t^k\boldsymbol{\beta}^k \\ \text{sym} & \boldsymbol{\beta}^k\mathbf{D}_t^k\boldsymbol{\beta}^k \end{bmatrix} dh = \begin{bmatrix} \mathbf{D}_t^{11} & \mathbf{D}_t^{12} \\ \text{sym} & \mathbf{D}_t^{22} \end{bmatrix} \tag{33}$$

where a standard term from the FSDT appears

$$\mathbf{D}_t^{11} = \int_h \mathbf{D}_t^k dh \tag{34}$$

while in the counter-diagonal:

$$\mathbf{D}_t^{12} = \int_h \mathbf{D}_t^k\boldsymbol{\beta}^k dh = \int_h \begin{bmatrix} G_{xx}^k & G_{xy}^k \\ G_{xy}^k & G_{yy}^k \end{bmatrix} \begin{bmatrix} \frac{G_x}{G_{xx}^k} - 1 & \\ & \frac{G_y}{G_{yy}^k} - 1 \end{bmatrix} dz \tag{35}$$

and finally

$$\mathbf{D}_t^{22} = \int_h \boldsymbol{\beta}^k\mathbf{D}_t^k\boldsymbol{\beta}^k dz = \int_h \begin{bmatrix} \frac{G_x}{G_{xx}^k} - 1 & \\ & \frac{G_y}{G_{yy}^k} - 1 \end{bmatrix} \begin{bmatrix} G_{xx}^k & G_{xy}^k \\ G_{xy}^k & G_{yy}^k \end{bmatrix} \begin{bmatrix} \frac{G_x}{G_{xx}^k} - 1 & \\ & \frac{G_y}{G_{yy}^k} - 1 \end{bmatrix} dz \tag{36}$$

Then the internal strain energy can be written as:

$$W = \frac{1}{2}\left(\boldsymbol{\varepsilon}_p^T\mathbf{D}_p\boldsymbol{\varepsilon}_p + \boldsymbol{\varepsilon}_t^T\mathbf{D}_t\boldsymbol{\varepsilon}_t\right) \tag{37}$$

that allows to define conjugated generalized stresses integrated across the thickness

$$\begin{bmatrix} (\boldsymbol{\sigma}_p)_{10\times1} \\ (\boldsymbol{\sigma}_t)_{4\times1} \end{bmatrix} = \begin{bmatrix} (\mathbf{D}_p)_{10\times10} & \mathbf{0} \\ \mathbf{0} & (\mathbf{D}_t)_{4\times4} \end{bmatrix} \begin{bmatrix} (\boldsymbol{\varepsilon}_p)_{10\times1} \\ (\boldsymbol{\varepsilon}_t)_{4\times1} \end{bmatrix} \qquad \boldsymbol{\sigma}_{14\times1} = \mathbf{D}_{14\times14}\boldsymbol{\varepsilon}_{14\times1} \tag{38}$$

The integrals in thickness are (denoting $\bar{z}_k = \frac{1}{2}(z_{k+1} + z_k)$ and $\bar{\boldsymbol{\Phi}}^k = \frac{1}{2}(\boldsymbol{\Phi}^{k+1} + \boldsymbol{\Phi}^k)$):

$$\begin{aligned} &\mathbf{D}_p^{11} = \sum_{k=1}^{NL}\mathbf{D}_p^k h_k \quad \mathbf{D}_p^{12} = \sum_{k=1}^{NL}\mathbf{D}_p^k h_k\bar{z}_k \quad \mathbf{D}_p^{13} = \sum_{k=1}^{NL}\mathbf{D}_p^k h_k\bar{\boldsymbol{\Phi}}^k \\ &\mathbf{D}_p^{22} = \sum_{k=1}^{NL}\mathbf{D}_p^k h_k\left(\bar{z}_k^2 + \frac{h_k^2}{12}\right) \quad \mathbf{D}_p^{23} = \sum_{k=1}^{NL}\mathbf{D}_p^k h_k\left[\bar{\boldsymbol{\Phi}}^k\bar{z}_k + \boldsymbol{\beta}^k\frac{h_k^2}{12}\right] \\ &\mathbf{D}_p^{33} = \sum_{k=1}^{NL} h_k\left[(\bar{\boldsymbol{\Phi}}^k)^T\mathbf{D}_p^k\bar{\boldsymbol{\Phi}}^k + \left(\boldsymbol{\beta}^k\right)^T\mathbf{D}_p^k\boldsymbol{\beta}^k\frac{h_k^2}{12}\right] \end{aligned} \tag{39}$$

$$\mathbf{D}_t^{11} = \sum_{k=1}^{NL}\mathbf{D}_t^k h_k \quad \mathbf{D}_t^{12} = \sum_{k=1}^{NL}\mathbf{D}_t^k h_k\boldsymbol{\beta}^k \quad \mathbf{D}_t^{22} = \sum_{k=1}^{NL}\left(\boldsymbol{\beta}^k\right)^T\mathbf{D}_t^k h_k\boldsymbol{\beta}^k \tag{40}$$

The resultant stress measures are

$$\begin{bmatrix} \boldsymbol{\sigma}_p \\ \boldsymbol{\sigma}_t \end{bmatrix} = \begin{bmatrix} \mathbf{D}_p & \mathbf{0} \\ \mathbf{0} & \mathbf{D}_t \end{bmatrix} \begin{bmatrix} \boldsymbol{\varepsilon}_p \\ \boldsymbol{\varepsilon}_t \end{bmatrix}$$

$$\begin{bmatrix} \mathbf{N} \\ \mathbf{M} \\ \mathbf{M}_\phi \\ \mathbf{Q} \\ \mathbf{Q}_\phi \end{bmatrix} = \begin{bmatrix} \begin{bmatrix} \mathbf{D}_p^{11} & \mathbf{D}_p^{12} & \mathbf{D}_p^{13} \\ & \mathbf{D}_p^{22} & \mathbf{D}_p^{23} \\ \text{sym} & & \mathbf{D}_p^{33} \end{bmatrix} & \mathbf{0} \\ \mathbf{0} & \begin{bmatrix} \mathbf{D}_t^{11} & \mathbf{D}_t^{12} \\ \text{sym} & \mathbf{D}_t^{22} \end{bmatrix} \end{bmatrix} \begin{bmatrix} \mathbf{E}_m \\ \boldsymbol{\chi} \\ \nabla\psi \\ \boldsymbol{\gamma} \\ \boldsymbol{\psi} \end{bmatrix} \tag{41}$$

It can be easily shown that

$$\mathbf{N} = \int_h \mathbf{D}_p\mathbf{E}dz = \int_h \boldsymbol{\sigma}_p dz \tag{42}$$

$$\mathbf{M} = \int_h z\mathbf{D}_p\mathbf{E}dz = \int_h z\boldsymbol{\sigma}_p dz \tag{43}$$

$$\mathbf{Q} = \int_h \mathbf{D}_t(\boldsymbol{\gamma} + \boldsymbol{\beta}\boldsymbol{\psi})dz = \int_h \boldsymbol{\tau}dz \tag{44}$$

represent what is usually meant by membrane, flexional and shear forces. While there are two new stress measures

$$\mathbf{M}_\phi = \mathbf{D}_p^{31}\mathbf{E}_m + \mathbf{D}_p^{32}\boldsymbol{\chi} + \mathbf{D}_p^{33}\nabla\boldsymbol{\psi} = \int_h \boldsymbol{\phi}^T\boldsymbol{\sigma}_p dz \tag{45}$$

$$\mathbf{Q}_\phi = \mathbf{D}_t^{21}\boldsymbol{\gamma} + \mathbf{D}_t^{22}\boldsymbol{\psi} = \int_h \boldsymbol{\beta}^T\boldsymbol{\tau}dz \tag{46}$$

associated with the in-plane and transverse direction gradient of function $\boldsymbol{\psi}$ respectively.

6. Shell elements

6.1. Configuration and local systems

The element configuration is defined by the position of the middle surface $\boldsymbol{\varphi}$ and the direction of the director $\mathbf{t}$, both with respect to a global system and the additional displacement field $\boldsymbol{\psi}$ in the local convective system. At any time the configuration results from the interpolation of the nodal values

$$\boldsymbol{\varphi} = \sum_{I=1}^{NN} N^I\boldsymbol{\varphi}^I \tag{47}$$

$$\mathbf{t} = \sum_{I=1}^{NN} N^I\mathbf{t}^I \tag{48}$$

$$\boldsymbol{\psi} = \sum_{I=1}^{NN} N^I\boldsymbol{\psi}^I \tag{49}$$

besides, the director $\mathbf{t}$ is part of a local triad where the other two vectors do not necessarily lay in the tangent plane to the shell middle surface

$$\boldsymbol{\Lambda} = [\,\mathbf{t}_1 \quad \mathbf{t}_2 \quad \mathbf{t}_3\,] \tag{50}$$

In the original configuration (index 0), at each integration point, a local orthogonal system $\left[\boldsymbol{\varphi}_x, \boldsymbol{\varphi}_y\right]_0^G$ is defined laying in the tangent plane to the shell middle surface. In a similar way at each mesh node a local system must be defined $\left[\boldsymbol{\varphi}_x, \boldsymbol{\varphi}_y\right]_0^I$ that can be related to the local nodal system $[\mathbf{t}_1, \mathbf{t}_2]_0^I$, first by an angle β between $\mathbf{t}_3$ and the normal to the tangent plane $\boldsymbol{\varphi}_x \times \boldsymbol{\varphi}_y$ and second by an angle α (a rotation around $\mathbf{t}_3$ of the local system to fit the nodal system) between $\boldsymbol{\varphi}_x$ and $\mathbf{t}_1$ that later allows to transform the contributions to the DoFs $\boldsymbol{\psi}$ from one nodal system to the other. The hierarchical nodal DoFs are then related at each node by

$$\begin{bmatrix} \psi_x \\ \psi_y \end{bmatrix}^I = \begin{bmatrix} \cos\alpha & \sin\alpha \\ -\sin\alpha & \cos\alpha \end{bmatrix}^I \begin{bmatrix} \psi_1 \\ \psi_2 \end{bmatrix}^I \qquad \boldsymbol{\psi}_L^I = \mathbf{R}_I\boldsymbol{\psi}_G^I \tag{51}$$

that must be used to compute the contributions to equilibrium equations and stiffness matrix.

Two elements have been considered in this work, namely a four-node bi-linear quadrilateral (`QL`) and a six-node triangle (`TLLL`) where middle surface geometry $\boldsymbol{\varphi}$ is linearly interpolated from the vertex nodes and the local system $\boldsymbol{\Lambda}$ is linearly interpolated from the mid-side nodes. For the additional in-plane displacements $\boldsymbol{\psi}$ the same interpolation of the middle surface is used.

6.2. Strains

The interpolation of the new variable $\boldsymbol{\psi}$ can be written in terms of the matrix

$$\Xi = \begin{bmatrix} N^1 & & & N^{NN} & \\ & N^1 & \dots & & N^{NN} \end{bmatrix}_{2\times2NN} \tag{52}$$

$$\boldsymbol{\psi} = \boldsymbol{\Xi}\boldsymbol{\psi}^e \tag{53}$$

where $\boldsymbol{\psi}^e$ includes the hierarchical nodal variables associated to the element. There are two new strain measures to compute and their respective tangent matrices:

- The in-plane gradient of $\boldsymbol{\psi}$ that is written as a four component column array

$$\begin{bmatrix} \psi_{x'x} \\ \psi_{y'y} \\ \psi_{x'y} \\ \psi_{y'x} \end{bmatrix} = \begin{bmatrix} N_x^1 & & \dots & N_x^{NN} & \\ & N_y^1 & & & N_y^{NN} \\ N_y^1 & & & N_y^{NN} & \\ & N_x^1 & & & N_x^{NN} \end{bmatrix} \boldsymbol{\psi}^e \tag{54}$$

$$\nabla\boldsymbol{\psi} = \mathbf{B}_{b\phi}\boldsymbol{\psi}^e$$

- The derivative in the transverse direction

$$\begin{bmatrix} \gamma_{\phi x} \\ \gamma_{\phi y} \end{bmatrix} = \begin{bmatrix} \beta_x \psi_x \\ \beta_y \psi_y \end{bmatrix} = \mathbf{B}_{s\phi}\boldsymbol{\psi}^e \tag{55}$$

Then the variation of all the strain measures can be written as (the expressions for the matrices $\mathbf{B}_m$, $\mathbf{B}_b$ and $\mathbf{B}_s$ may be found in the original papers [14,4])

$$\delta \begin{bmatrix} \mathbf{E}_m \\ \boldsymbol{\chi} \\ \nabla\psi \\ \boldsymbol{\gamma} \\ \boldsymbol{\psi} \end{bmatrix} = \begin{bmatrix} \mathbf{B}_m & & & \\ \mathbf{B}_b^1 & \mathbf{B}_b^2 & & \\ & & \mathbf{B}_{b\phi} & \\ \bar{\mathbf{B}}_s^1 & \bar{\mathbf{B}}_s^2 & & \\ & & \bar{\mathbf{B}}_{s\phi} & \end{bmatrix} \begin{bmatrix} \delta\mathbf{u} \\ \delta\mathbf{T} \\ \delta\boldsymbol{\psi} \end{bmatrix} \tag{56}$$

where $\delta\mathbf{u}_{3\times1}$ is the variation of the middle surface and $\delta\mathbf{T}_{2\times1}$ denotes the in-plane components of the director variation. Note also that an assumed natural strain (ANS) approach is used for transverse shear then $\mathbf{B}_s$ will be substituted by $\bar{\mathbf{B}}_s$ matrices as shown below.

The equivalent nodal forces stem from the integration at each element

$$\begin{bmatrix} \delta\mathbf{u} \\ \delta\mathbf{T} \\ \delta\boldsymbol{\psi} \end{bmatrix}^T \int_A \begin{bmatrix} \mathbf{B}_m & & & \\ \mathbf{B}_b^1 & \mathbf{B}_b^2 & & \\ & & \mathbf{B}_{b\phi} & \\ \bar{\mathbf{B}}_s^1 & \bar{\mathbf{B}}_s^2 & & \\ & & \bar{\mathbf{B}}_{s\phi} & \end{bmatrix}^T \begin{bmatrix} \mathbf{N} \\ \mathbf{M} \\ \mathbf{M}_\phi \\ \mathbf{Q} \\ \mathbf{Q}_\phi \end{bmatrix} dA \tag{57}$$

that is numerically performed with *NG* points with weighting coefficients *w*. The contributions may be split in two parts

1. that corresponding to membrane and bending forces

$$\begin{bmatrix} \delta\mathbf{u} \\ \delta\mathbf{T} \\ \delta\boldsymbol{\psi} \end{bmatrix}^T \sum_{G=1}^{NG} \begin{bmatrix} \mathbf{B}_m & & & \\ \mathbf{B}_b^1 & \mathbf{B}_b^2 & & \\ & & \mathbf{B}_{b\phi} & \end{bmatrix}_G^T \begin{bmatrix} \mathbf{N} \\ \mathbf{M} \\ \mathbf{M}_\phi \end{bmatrix}_G J_G w_G \tag{58}$$

2. that corresponding to transverse shear forces

$$\begin{bmatrix} \delta\mathbf{u} \\ \delta\mathbf{T} \\ \delta\boldsymbol{\psi} \end{bmatrix}^T \sum_{G=1}^{NG} \begin{bmatrix} \bar{\mathbf{B}}_s^1 & \bar{\mathbf{B}}_s^2 & & \\ & & \bar{\mathbf{B}}_{s\phi} & \end{bmatrix}^T \begin{bmatrix} \mathbf{Q} \\ \mathbf{Q}_\phi \end{bmatrix} J_G w_G \tag{59}$$

where the substitute matrices $\bar{\mathbf{B}}_s$ and $\bar{\mathbf{B}}_{s\phi}$ are obtained by interpolation of matrices computed at sampling points (see next section).

7. Transverse shear approach

In the original version of the elements an ANS approach has been used for transverse shear strains leading to substitute matrices ($\bar{\mathbf{B}}_s$). In the same line it is possible to define an almost identical approach for $\bar{\mathbf{B}}_{s\phi}$ assuming the same interpolation for these new shear strains in natural coordinates. Let us see the details for both elements.

7.1. Four-node quadrilateral QL

For the four-node quadrilateral function $\boldsymbol{\psi}$ is re-interpolated from four sampling points located ad mid-side points

$$\bar{\boldsymbol{\psi}} = \begin{bmatrix} \psi_\xi \\ \psi_\eta \end{bmatrix} = \frac{1}{2} \begin{bmatrix} 0 & 1-\eta & 0 & 1+\eta \\ 1-\xi & 0 & 1+\xi & 0 \end{bmatrix} \begin{bmatrix} \psi_\eta^A \\ \psi_\xi^B \\ \psi_\eta^C \\ \psi_\xi^D \end{bmatrix} = \mathbf{P}(\xi,\eta)\ \tilde{\boldsymbol{\psi}} \tag{60}$$

where the values of function $\boldsymbol{\psi}$ at the sampling points in terms of the nodal values are

$$\begin{bmatrix} \boldsymbol{\psi}^A \\ \boldsymbol{\psi}^B \\ \boldsymbol{\psi}^C \\ \boldsymbol{\psi}^D \end{bmatrix} = \frac{1}{2} \begin{bmatrix} \mathbf{1} & & & \mathbf{1} \\ \mathbf{1} & \mathbf{1} & & \\ & \mathbf{1} & \mathbf{1} & \\ & & \mathbf{1} & \mathbf{1} \end{bmatrix} \begin{bmatrix} \boldsymbol{\psi}^1 \\ \boldsymbol{\psi}^2 \\ \boldsymbol{\psi}^3 \\ \boldsymbol{\psi}^4 \end{bmatrix} \tag{61}$$

The covariant components of function $\boldsymbol{\psi}$ respect to the natural system (ξ,η) are obtained projecting on vectors $\boldsymbol{\varphi}_\xi$ and $\boldsymbol{\varphi}_\eta$. Remind that the in-plane Jacobian matrix of the isoparametric mapping is:

$$\left[\boldsymbol{\varphi}_\xi, \boldsymbol{\varphi}_\eta\right] = \mathbf{J} \quad \left[\boldsymbol{\varphi}^\xi, \boldsymbol{\varphi}^\eta\right] = \left[\boldsymbol{\varphi}_\xi, \boldsymbol{\varphi}_\eta\right]^{-T} = \mathbf{J}^{-T} = \begin{bmatrix} \boldsymbol{\varphi}^\xi \cdot \mathbf{t}_x & \boldsymbol{\varphi}^\eta \cdot \mathbf{t}_x \\ \boldsymbol{\varphi}^\xi \cdot \mathbf{t}_y & \boldsymbol{\varphi}^\eta \cdot \mathbf{t}_y \end{bmatrix} \tag{62}$$

At the sampling points only the components along the sides are considered

$$\begin{bmatrix} \psi_\eta^A \\ \psi_\xi^B \\ \psi_\eta^C \\ \psi_\xi^D \end{bmatrix} = \begin{bmatrix} \boldsymbol{\varphi}_\xi^S \cdot \boldsymbol{\psi}^A \\ \boldsymbol{\varphi}_\xi^B \cdot \boldsymbol{\psi}^B \\ \boldsymbol{\varphi}_\xi^C \cdot \boldsymbol{\psi}^C \\ \boldsymbol{\varphi}_\xi^D \cdot \boldsymbol{\psi}^D \end{bmatrix} = \frac{1}{2} \begin{bmatrix} \left(\boldsymbol{\varphi}_\eta^A\right)^T & & & \left(\boldsymbol{\varphi}_\eta^A\right)^T \\ \left(\boldsymbol{\varphi}_\xi^B\right)^T & \left(\boldsymbol{\varphi}_\xi^B\right)^T & & \\ & \left(\boldsymbol{\varphi}_\eta^C\right)^T & \left(\boldsymbol{\varphi}_\eta^C\right)^T & \\ & & \left(\boldsymbol{\varphi}_\xi^D\right)^T & \left(\boldsymbol{\varphi}_\xi^D\right)^T \end{bmatrix} \begin{bmatrix} \boldsymbol{\psi}^1 \\ \boldsymbol{\psi}^2 \\ \boldsymbol{\psi}^3 \\ \boldsymbol{\psi}^4 \end{bmatrix}$$

$$\tilde{\boldsymbol{\psi}} = \mathbf{T}_{4\times8}\boldsymbol{\psi}^e \tag{63}$$

that substituted in Eq. (60)

$$\bar{\boldsymbol{\psi}} = \mathbf{P}(\xi,\eta)\ \mathbf{T}\ \boldsymbol{\psi}^e \tag{64}$$

allows to rebuild the vector

$$\boldsymbol{\psi} = \bar{\psi}_\xi \boldsymbol{\varphi}^\xi + \bar{\psi}_\eta \boldsymbol{\varphi}^\eta \tag{65}$$

that is evaluated at the integration points where the Cartesian convective components are recovered

$$\begin{bmatrix} \psi_x \\ \psi_y \end{bmatrix}^G = \begin{bmatrix} \mathbf{t}_x \cdot \boldsymbol{\varphi}^\xi & \mathbf{t}_x \cdot \boldsymbol{\varphi}^\eta \\ \mathbf{t}_y \cdot \boldsymbol{\varphi}^\xi & \mathbf{t}_y \cdot \boldsymbol{\varphi}^\eta \end{bmatrix}^G \begin{bmatrix} \bar{\psi}_\xi \\ \bar{\psi}_\eta \end{bmatrix}^G = \mathbf{J}_G^{-T}\ \mathbf{P}(\xi_G,\eta_G)\ \mathbf{T}\ \boldsymbol{\psi}^e \tag{66}$$

The associated equivalent nodal forces are obtained by the integral

$$\int_A \mathbf{B}_{s\phi}^T \mathbf{Q}_\phi dA = \mathbf{T}^T \int_A \mathbf{P}^T(\xi_G,\eta_G)\ \mathbf{J}_G^{-1} \mathbf{Q}_\phi dA = \frac{1}{4} \begin{bmatrix} \boldsymbol{\varphi}_\eta^A & \boldsymbol{\varphi}_\xi^B & & \\ & \boldsymbol{\varphi}_\xi^B & \boldsymbol{\varphi}_\eta^C & \\ & & \boldsymbol{\varphi}_\eta^C & \boldsymbol{\varphi}_\xi^D \\ \boldsymbol{\varphi}_\eta^A & & & \boldsymbol{\varphi}_\xi^D \end{bmatrix} \sum_{G=1}^{NG} \mathbf{P}^T \mathbf{J}_G^{-1} \mathbf{Q}_\phi J_G w_G \tag{67}$$

where it can be defined

$$(\mathbf{q}_\phi)_{4\times1} = \frac{1}{2}\sum_{G=1}^{NG}\mathbf{P}^T\mathbf{J}_G^{-1}\mathbf{Q}_\phi J_G w_G \tag{68}$$

then

$$\int_A \mathbf{B}_{s\phi}^T\mathbf{Q}_\phi dA = \mathbf{T}^T\mathbf{q}_\phi \tag{69}$$

7.2. Six-node linear triangle TLLL

For this six-node triangle with linear interpolation of both the middle surface ($\boldsymbol{\varphi}$ and $\boldsymbol{\psi}$) and the director field, to deal with transverse shear the function $\boldsymbol{\psi}$ is re-interpolated from three sampling points located at mid-sides. Besides, for a linear triangle, strain and stresses (transverse shear included) are computed at the element center only. To avoid an excessively flexible element due to sub-integration, which leads to the appearance of a shear spurious mode, it is desirable to use some form of stabilization. It is therefore convenient to write in parallel:

$$\bar{\boldsymbol{\gamma}} = \begin{bmatrix}\gamma_\xi\\ \gamma_\eta\end{bmatrix} = \begin{bmatrix}-\eta & -\eta & 1-\eta\\ \xi & \xi-1 & \xi\end{bmatrix}\begin{bmatrix}\sqrt{2}\gamma_t^4\\ -\gamma_\eta^5\\ \gamma_\xi^6\end{bmatrix} = \mathbf{P}(\xi,\eta)\ \tilde{\boldsymbol{\gamma}} \tag{70}$$

$$\bar{\boldsymbol{\psi}} = \begin{bmatrix}\psi_\xi\\ \psi_\eta\end{bmatrix} = \begin{bmatrix}-\eta & -\eta & 1-\eta\\ \xi & \xi-1 & \xi\end{bmatrix}\begin{bmatrix}\sqrt{2}\psi_t^4\\ -\psi_\eta^5\\ \psi_\xi^6\end{bmatrix} = \mathbf{P}(\xi,\eta)\ \tilde{\boldsymbol{\psi}} \tag{71}$$

in this case the $\tilde{\boldsymbol{\psi}}$ are the components along each side evaluated at mid-side nodes. The covariant components of the function $\boldsymbol{\psi}$ with respect to the natural system (ξ,η) are obtained projecting in directions $\boldsymbol{\varphi}_\xi$ y $\boldsymbol{\varphi}_\eta$. Then

$$\begin{bmatrix}\sqrt{2}\gamma_t^4\\ -\gamma_\eta^5\\ \gamma_\xi^6\end{bmatrix} = \begin{bmatrix}\sqrt{2}\boldsymbol{\varphi}_t^4\cdot\mathbf{t}^4\\ -\boldsymbol{\varphi}_\eta^5\cdot\mathbf{t}^5\\ \boldsymbol{\varphi}_\xi^6\cdot\mathbf{t}^6\end{bmatrix} \tag{72}$$

$$\begin{bmatrix}\sqrt{2}\psi_t^4\\ -\psi_\eta^5\\ \psi_\xi^6\end{bmatrix} = \frac{1}{2}\begin{bmatrix}\sqrt{2}\boldsymbol{\varphi}_t^4\cdot(\boldsymbol{\psi}^2+\boldsymbol{\psi}^3)\\ -\boldsymbol{\varphi}_\eta^5\cdot(\boldsymbol{\psi}^3+\boldsymbol{\psi}^1)\\ \boldsymbol{\varphi}_\xi^6\cdot(\boldsymbol{\psi}^1+\boldsymbol{\psi}^2)\end{bmatrix} \tag{73}$$

with the difference that in the first case the inner products are in 3D space and both vectors are changing during the deformation process, whereas in the second case it is in the 2D space tangent to the shell and the tangent vectors to the side are unchangeable due to the nature of the approximation. At each point of interest the interpolation allows to reconstruct the vectors

$$\boldsymbol{\gamma} = \bar{\gamma}_\xi\boldsymbol{\varphi}^\xi + \bar{\gamma}_\eta\boldsymbol{\varphi}^\eta \tag{74}$$

$$\boldsymbol{\psi} = \bar{\psi}_\xi\boldsymbol{\varphi}^\xi + \bar{\psi}_\eta\boldsymbol{\varphi}^\eta \tag{75}$$

which are used in the integration points where Cartesian components are recovered

$$\begin{bmatrix}\gamma_x\\ \gamma_y\end{bmatrix}^G = \begin{bmatrix}\mathbf{t}_x\cdot\bar{\boldsymbol{\gamma}}\\ \mathbf{t}_y\cdot\bar{\boldsymbol{\gamma}}\end{bmatrix}^G = \begin{bmatrix}\mathbf{t}_x\cdot\boldsymbol{\varphi}^\xi & \mathbf{t}_x\cdot\boldsymbol{\varphi}^\eta\\ \mathbf{t}_y\cdot\boldsymbol{\varphi}^\xi & \mathbf{t}_y\cdot\boldsymbol{\varphi}^\eta\end{bmatrix}\begin{bmatrix}\bar{\gamma}_\xi\\ \bar{\gamma}_\eta\end{bmatrix} = \mathbf{J}^{-T}\ \mathbf{P}(\xi_G,\eta_G)\ \tilde{\boldsymbol{\gamma}} \tag{76}$$

$$\begin{bmatrix}\psi_x\\ \psi_y\end{bmatrix}^G = \begin{bmatrix}\mathbf{t}_x\cdot\bar{\boldsymbol{\psi}}\\ \mathbf{t}_y\cdot\bar{\boldsymbol{\psi}}\end{bmatrix}^G = \begin{bmatrix}\mathbf{t}_x\cdot\boldsymbol{\varphi}^\xi & \mathbf{t}_x\cdot\boldsymbol{\varphi}^\eta\\ \mathbf{t}_y\cdot\boldsymbol{\varphi}^\xi & \mathbf{t}_y\cdot\boldsymbol{\varphi}^\eta\end{bmatrix}\begin{bmatrix}\bar{\psi}_\xi\\ \bar{\psi}_\eta\end{bmatrix} = \mathbf{J}^{-T}\ \mathbf{P}(\xi_G,\eta_G)\ \tilde{\boldsymbol{\psi}} \tag{77}$$

7.2.1. Equivalent nodal forces due to transverse shear

The nodal forces associated with the standard transverse shear are obtained by the integral

$$\mathbf{r} = \int_A [\bar{\mathbf{B}}_s]_{2\times15}^T\begin{bmatrix}Q_1\\ Q_2\end{bmatrix}dA = \int_A \left[\tilde{\mathbf{B}}_s\right]_{3\times15}^T\mathbf{P}^T\mathbf{J}^{-1}\mathbf{Q}dA = \left[\tilde{\mathbf{B}}_s\right]_{3\times15}^T\bar{\mathbf{Q}} \tag{78}$$

where a vector $\bar{\mathbf{Q}}$ associated to shear forces has been defined and will be called "integrated shear force vector". In the elastic case is the sum of:

$$\bar{\mathbf{Q}}_{3\times1}^1 = \int_A \mathbf{P}^T\bar{\mathbf{D}}_t^{11}\mathbf{P}dA\begin{bmatrix}\sqrt{2}\gamma_{rt}^4\\ -\gamma_{r\eta}^5\\ \gamma_{r\xi}^6\end{bmatrix} \tag{79}$$

$$\bar{\mathbf{Q}}_{3\times1}^2 = \int_A \mathbf{P}^T\bar{\mathbf{D}}_t^{12}\mathbf{P}dA\begin{bmatrix}\sqrt{2}\psi_t^4\\ -\psi_\eta^5\\ \psi_\xi^6\end{bmatrix} \tag{80}$$

with

$$\bar{\mathbf{D}}_t^{ij} = \mathbf{J}^{-1}\bar{\mathbf{D}}_t^{ij}\mathbf{J}^{-T} = \begin{bmatrix}a & c\\ c & b\end{bmatrix}^{ij} \tag{81}$$

Explicitly integrating in the area

$$\begin{aligned}\bar{\mathbf{Q}}_{3\times1} &= \frac{A}{6}\begin{bmatrix}a+b-c & a-b+c & -a+b+c\\ & a+3b+3c & -a-b-3c\\ sim. & & 3a+b+3c\end{bmatrix}^{11}\begin{bmatrix}\sqrt{2}\gamma_{rt}^4\\ -\gamma_{r\eta}^5\\ \gamma_{r\xi}^6\end{bmatrix}\\ &+\frac{A}{6}\begin{bmatrix}a+b-c & a-b+c & -a+b+c\\ & a+3b+3c & -a-b-3c\\ sim. & & 3a+b+3c\end{bmatrix}^{12}\begin{bmatrix}\sqrt{2}\psi_t^4\\ -\psi_\eta^5\\ \psi_\xi^6\end{bmatrix}\\ &= \tilde{\mathbf{D}}_t^{11}\begin{bmatrix}\sqrt{2}\gamma_{rt}^4\\ -\gamma_{r\eta}^5\\ \gamma_{r\xi}^6\end{bmatrix} + \tilde{\mathbf{D}}_t^{12}\begin{bmatrix}\sqrt{2}\psi_t^4\\ -\psi_\eta^5\\ \psi_\xi^6\end{bmatrix}\end{aligned} \tag{82}$$

Similarly a vector $\bar{\mathbf{Q}}_\phi$ can be defined as

$$\mathbf{r}_\phi = \int_A [\bar{\mathbf{B}}_{\phi s}]_{2\times6}^T\begin{bmatrix}Q_{\phi1}\\ Q_{\phi2}\end{bmatrix}dA = \int_A \left[\tilde{\mathbf{B}}_{\phi s}\right]_{3\times6}^T\mathbf{P}^T\mathbf{J}^{-1}\mathbf{Q}_\phi dA = \left[\tilde{\mathbf{B}}_{\phi s}\right]_{3\times6}^T\bar{\mathbf{Q}}_\phi \tag{83}$$

that in elastic case is the sum of

$$\bar{\mathbf{Q}}_{\phi3\times1}^1 = \int_A \mathbf{P}^T\bar{\mathbf{D}}_t^{21}\mathbf{P}dA\begin{bmatrix}\sqrt{2}\gamma_{rt}^4\\ -\gamma_{r\eta}^5\\ \gamma_{r\xi}^6\end{bmatrix} \tag{84}$$

$$\bar{\mathbf{Q}}_{\phi3\times1}^2 = \int_A \mathbf{P}^T\bar{\mathbf{D}}_t^{22}\mathbf{P}dA\begin{bmatrix}\sqrt{2}\psi_t^4\\ -\psi_\eta^5\\ \psi_\xi^6\end{bmatrix} \tag{85}$$

Explicitly integrating in the area

$$\begin{aligned}\bar{\mathbf{Q}}_{3\times1} &= \frac{A}{6}\begin{bmatrix}a+b-c & a-b+c & -a+b+c\\ & a+3b+3c & -a-b-3c\\ sim. & & 3a+b+3c\end{bmatrix}^{21}\begin{bmatrix}\sqrt{2}\gamma_{rt}^4\\ -\gamma_{r\eta}^5\\ \gamma_{r\xi}^6\end{bmatrix}\\ &+\frac{A}{6}\begin{bmatrix}a+b-c & a-b+c & -a+b+c\\ & a+3b+3c & -a-b-3c\\ sim. & & 3a+b+3c\end{bmatrix}^{22}\begin{bmatrix}\sqrt{2}\psi_t^4\\ -\psi_\eta^5\\ \psi_\xi^6\end{bmatrix}\\ &= \tilde{\mathbf{D}}_t^{21}\begin{bmatrix}\sqrt{2}\gamma_{rt}^4\\ -\gamma_{r\eta}^5\\ \gamma_{r\xi}^6\end{bmatrix} + \tilde{\mathbf{D}}_t^{22}\begin{bmatrix}\sqrt{2}\psi_t^4\\ -\psi_\eta^5\\ \psi_\xi^6\end{bmatrix}\end{aligned} \tag{86}$$

Thus material stiffness matrix associated to transverse shear results:

$$\mathbf{K}_s^M = \begin{bmatrix} \tilde{\mathbf{B}}_s & \\ & \tilde{\mathbf{B}}_{\phi s} \end{bmatrix}^T \begin{bmatrix} \tilde{\mathbf{D}}_t^{11} & \tilde{\mathbf{D}}_t^{11} \\ \tilde{\mathbf{D}}_t^{21} & \tilde{\mathbf{D}}_t^{22} \end{bmatrix} \begin{bmatrix} \tilde{\mathbf{B}}_s & \\ & \tilde{\mathbf{B}}_{\phi s} \end{bmatrix} \tag{87}$$

7.2.2. Shear stabilization

In case a single integration point at the center of the element is used, it is necessary to stabilize the shear to avoid the appearance of spurious modes without associated strain energy. To achieve this, natural shear strains are first written as the sum

$$\begin{bmatrix} \gamma_\xi \\ \gamma_\eta \end{bmatrix} = \left\{ \begin{bmatrix} -\frac{1}{3} & -\frac{1}{3} & \frac{2}{3} \\ \frac{1}{3} & -\frac{2}{3} & \frac{1}{3} \end{bmatrix} + \begin{bmatrix} -\eta+\frac{1}{3} & -\eta+\frac{1}{3} & \frac{1}{3}-\eta \\ \xi-\frac{1}{3} & \xi-\frac{1}{3} & \xi-\frac{1}{3} \end{bmatrix} \right\} \begin{bmatrix} \sqrt{2}\gamma_t^4 \\ -\gamma_\eta^5 \\ \gamma_\xi^6 \end{bmatrix}$$
$$= [\mathbf{P}_C + \mathbf{P}_H]\boldsymbol{\gamma}' = \begin{bmatrix} \gamma_\xi \\ \gamma_\eta \end{bmatrix}_C + \begin{bmatrix} \gamma_\xi \\ \gamma_\eta \end{bmatrix}_H \tag{88}$$

The first component corresponds to values at the element center (subscript "C") and the second component (subscript "H"), which vanishes in the center and varies linearly, can be used to perform the required stabilization. Similarly the additional shear strain

$$\begin{bmatrix} \psi_\xi \\ \psi_\eta \end{bmatrix} = [\mathbf{P}_C + \mathbf{P}_H]\boldsymbol{\psi}' = \begin{bmatrix} \psi_\xi \\ \psi_\eta \end{bmatrix}_C + \begin{bmatrix} \psi_\xi \\ \psi_\eta \end{bmatrix}_H \tag{89}$$

The integrated shear force vectors are split similarly

$$\bar{\mathbf{Q}}_{3\times1} = \bar{\mathbf{Q}}_{3\times1}^C + \bar{\mathbf{Q}}_{3\times1}^H \tag{90}$$
$$\bar{\mathbf{Q}}_{\phi3\times1} = \bar{\mathbf{Q}}_{\phi3\times1}^C + \bar{\mathbf{Q}}_{\phi3\times1}^H \tag{91}$$

with the component evaluated at the center

$$\bar{\mathbf{Q}}_{3\times1}^C = A\mathbf{P}_C\mathbf{J}^{-1}\mathbf{Q}_C \tag{92}$$
$$\bar{\mathbf{Q}}_{\phi3\times1}^C = A\mathbf{P}_C\mathbf{J}^{-1}\mathbf{Q}_{\phi C} \tag{93}$$

The shear strain components $\boldsymbol{\gamma}'_H$ and $\boldsymbol{\psi}'_H$ can be used in various ways for stabilization. Within an implicit scheme the non-constant part of the integrated shear force vector can be written:

$$\bar{\mathbf{Q}}_{3\times1}^H = \int_A \mathbf{P}^T\mathbf{J}^{-1}\bar{\mathbf{D}}_t^{11}\mathbf{J}^{-T}\mathbf{P}_H dA \begin{bmatrix} \sqrt{2}\gamma_t^4 \\ -\gamma_\eta^5 \\ \gamma_\xi^6 \end{bmatrix} + \int_A \mathbf{P}^T\mathbf{J}^{-1}\bar{\mathbf{D}}_t^{12}\mathbf{J}^{-T}\mathbf{P}_H dA \begin{bmatrix} \sqrt{2}\psi_t^4 \\ -\psi_\eta^5 \\ \psi_\xi^6 \end{bmatrix}$$
$$= \int_A \mathbf{P}^T\tilde{\mathbf{D}}_t^{11}\mathbf{P}_H \, dA \, \boldsymbol{\gamma}' + \int_A \mathbf{P}_C^T\tilde{\mathbf{D}}_t^{12}\mathbf{P}_H \, dA \, \boldsymbol{\psi}' \tag{94}$$
$$\bar{\mathbf{Q}}_{\phi3\times1}^H = \int_A \mathbf{P}^T\tilde{\mathbf{D}}_t^{12}\mathbf{P}_H \, dA \, \boldsymbol{\gamma}' + \int_A \mathbf{P}_C^T\tilde{\mathbf{D}}_t^{22}\mathbf{P}_H \, dA \, \boldsymbol{\psi}' \tag{95}$$

Explicitly integrating in the area

$$\bar{\mathbf{Q}}_{3\times1}^H = \frac{A(a+b+c)^{11}}{18} \begin{bmatrix} 1 & 1 & 1 \\ 1 & 1 & 1 \\ 1 & 1 & 1 \end{bmatrix} \begin{bmatrix} \sqrt{2}\gamma_t^4 \\ -\gamma_\eta^5 \\ \gamma_\xi^6 \end{bmatrix} + \frac{A(a+b+c)^{12}}{18} \begin{bmatrix} 1 & 1 & 1 \\ 1 & 1 & 1 \\ 1 & 1 & 1 \end{bmatrix} \begin{bmatrix} \sqrt{2}\psi_t^4 \\ -\psi_\eta^5 \\ \psi_\xi^6 \end{bmatrix}$$
$$= \frac{A}{18}\Big[(a+b+c)^{11}\left(\sqrt{2}\gamma_t^4 - \gamma_\eta^5 + \gamma_\xi^6\right) + (a+b+c)^{12}\left(\sqrt{2}\psi_t^4 - \psi_\eta^5 + \psi_\xi^6\right)\Big] \begin{bmatrix} 1 \\ 1 \\ 1 \end{bmatrix} \tag{96}$$

$$\bar{\mathbf{Q}}_{\phi3\times1}^H = \frac{A}{18}\Big[(a+b+c)^{12}\left(\sqrt{2}\gamma_t^4 - \gamma_\eta^5 + \gamma_\xi^6\right) + (a+b+c)^{22}\left(\sqrt{2}\psi_t^4 - \psi_\eta^5 + \psi_\xi^6\right)\Big] \begin{bmatrix} 1 \\ 1 \\ 1 \end{bmatrix} \tag{97}$$

that can be written as:

$$\begin{bmatrix} \bar{\mathbf{Q}}_{3\times1}^H \\ \bar{\mathbf{Q}}_{\phi3\times1}^H \end{bmatrix} = \begin{bmatrix} \tilde{\mathbf{D}}^{H11} & \tilde{\mathbf{D}}^{H12} \\ \tilde{\mathbf{D}}^{H12} & \tilde{\mathbf{D}}^{H22} \end{bmatrix} \begin{bmatrix} \boldsymbol{\gamma}' \\ \boldsymbol{\psi}' \end{bmatrix} \tag{98}$$

where

$$\tilde{\mathbf{D}}^{Hij} = \frac{A(a+b+c)^{ij}}{18} \begin{bmatrix} 1 & 1 & 1 \\ & 1 & 1 \\ \text{sim.} & & 1 \end{bmatrix} \tag{99}$$

In this way the stiffness matrix associated to transverse shear stabilization results:

$$\mathbf{K}_s^H = \begin{bmatrix} \tilde{\mathbf{B}}_s & \\ & \tilde{\mathbf{B}}_{\phi s} \end{bmatrix}^T \begin{bmatrix} \tilde{\mathbf{D}}_t^{H11} & \tilde{\mathbf{D}}_t^{H12} \\ \tilde{\mathbf{D}}_t^{H21} & \tilde{\mathbf{D}}_t^{H22} \end{bmatrix}_{6\times6} \begin{bmatrix} \tilde{\mathbf{B}}_s & \\ & \tilde{\mathbf{B}}_{\phi s} \end{bmatrix} \tag{100}$$

While the material stiffness matrix with one integration point is:

$$\mathbf{K}_s^M = \begin{bmatrix} \tilde{\mathbf{B}}_s & \\ & \tilde{\mathbf{B}}_{\phi s} \end{bmatrix}^T \begin{bmatrix} \tilde{\mathbf{D}}_t^{C11} & \tilde{\mathbf{D}}_t^{C11} \\ \tilde{\mathbf{D}}_t^{C21} & \tilde{\mathbf{D}}_t^{C22} \end{bmatrix}_{6\times6} \begin{bmatrix} \tilde{\mathbf{B}}_s & \\ & \tilde{\mathbf{B}}_{\phi s} \end{bmatrix} \tag{101}$$

with

$$\tilde{\mathbf{D}}_s^{Cij} = \tilde{\mathbf{D}}_t^{ij} - \tilde{\mathbf{D}}^{Hij} = \frac{A}{9} \begin{bmatrix} a+b-2c & a-2b+c & -2a+b+c \\ & a+4b+4c & -2a-2b-5c \\ & & 4a+b+4c \end{bmatrix}^{ij} \tag{102}$$

8. Examples

The present examples are intended to show that the results of plate models match or converge to analytical results published in the literature for ZZRT, i.e. the objective is to validate the finite element model. It is not the purpose of this section (or work) to assess the ZZRT which has already been done by other authors, who have studied the profiles of displacements and stresses across the thickness of the laminate. Besides, when curved shells in nonlinear regime are considered it is necessary to compare with numerical models discretized with solid elements. In that case this section is intended to show that the deformations are broadly similar in both models which contributes significantly to the assessment of the ZZRT, but no detailed displacements or stresses profiles across the thickness of the laminate are compared here.

The materials involved in the examples analyzed below have the mechanical properties (E_I and G_{IJ} in GPa and density (ρ) in Kg/m^3) listed in Table 1. The table includes two rather stiff materials (1 and 4) used as the external layers of the laminates and three materials (2, 3 and 5) used as internal layers (core) of the laminates. The three laminates considered have five layers and are symmetric with respect to the middle surface. They are defined in Table 2 where α indicates the angle (in degrees) between the material axis 1 with local direction x. The thickness of each layer is expressed as percentage of the total thickness of the laminate.

8.1. Simple supported square plate under bi-sinusoidal load

This example was taken from [6], the cross section is defined by sandwich laminate 1 with total thickness $t = 0.5$ m. A simple sup-

Table 1
Material properties (E_I and G_{IJ} en GPa).

Mat	1	2	3	4	5 (iso)
E_1	50	10^{-5}	0.01	131	0.00689
E_2	10	10^{-5}	0.01	10.34	
E_3	10	0.07585	0.07585	10.34	
ν_{12}	0.05	0.01	0.01	0.22	0.00
ν_{13}	0.05	0.01	0.01	0.22	
ν_{23}	0.25	0.01	0.01	0.49	
G_{12}	5	0.0225	0.0225	6.895	
G_{13}	5	0.0225	0.0225	6.205	
G_{23}	5	0.0225	0.0225	6.895	
ρ	1000	1000	1000	1627	97

Table 2
Sandwich laminates stacking sequence.

Mat	t[%]	α
(1)		
1	5	0
1	5	90
2	80	0
1	5	90
1	5	0
(2)		
1	5	0
1	5	90
3	80	0
1	5	90
1	5	0
(3)		
4	4.1667	0
4	4.1666	90
5	83.334	0
4	4.1666	90
4	4.1667	0

ported square plate with side length $a = 10$ m (aspect ratio $a/h = 20$) is subjected to a bi-sinusoidal load (null on the border and maximum at the center) of amplitude $q_0 = 1$ KPa.

Due to symmetry one quarter of the plate is discretized where the center of the plate coincides with the origin of the coordinate system. The imposed boundary conditions are (“hard-type”):

Side	u	v	w	θ_x	θ_y	ψ_x	ψ_y
$x = 0$	0.0				0.0	0.0	
$y = 0$		0.0		0.0			0.0
$x = a/2$	0.0	0.0	0.0	0.0			0.0
$y = a/2$	0.0	0.0	0.0		0.0	0.0	

A uniform structured mesh with an equal step in both directions $\Delta = 0.15625$ m was considered, that implies 33 nodes per side, a total of 1089 nodes and 1024 four-node quadrilateral elements (QL) or 512 six-node triangular elements (TLLL).

The vertical displacement at the plate center computed according to Reference [6] is

$$w(0,0) = 0.1118 \times \frac{D_{11}}{a^4} q_0 = 0.6742 \text{ mm}$$

Using element QL (7232 DoFs) it gets 0.6740 (99.96%) and with element TLLL (2848 DoFs) it gets 0.6752 (100.14%) that is slightly larger that the reference value, which may be associated to the non-conformity of the director field. Note that the model with elements QL has 2.5 times the number of DoFs of the model with TLLL elements. On the other hand a plot of stress states from the integration points are much smoother using the quadrilateral element so this is generally preferred if a structured mesh is possible. Considering the first-order theory (FSDT), the theoretical value is 0.2472 and those obtained by the finite element models are respectively 0.2469 (99.86%) and 0.2483 (100.41%), slightly below and above the reference value. In Fig. 1 the amplitude of the additional displacement is shown for the two elements considered.

8.2. Clamped plate under uniform load

The same geometry but fully clamped at the edges was analyzed but now under a uniform load $q = 1$ KPa. The maximum displacement obtained was $w_{max}^{QL} = 0.6916$ with the QL model and $w_{max}^{TLLL} = 0.6985$ with the TLLL model. In this case comparison is made against a finite element model with 20-node standard solid elements and a mesh of $16 \times 16 \times 9$ (one element per layer in the outer layers and 5 elements in the core). For the latter model the displacement computed was $w_{max}^{Solid} = 0.6936$ (average of top and bottom surfaces) that shows a very good correlation between the shell and the solid model. On the other hand using the FSDT the displacement computed at the center is just $w_{max}^{FSDT} = 0.1134$.

8.3. Vibration of a square plate

To assess simple dynamic behavior natural frequencies of a simply supported square plate have been computed that can be compared with recently published results [6]. Two aspect ratios where considered, namely $a/t = 10$ and $a/t = 100$, and the sandwich laminate 3 was used for the transverse section. The same discretization of the first example was used again (with symmetry conditions) so it is only possible to evaluate symmetric modes. A simple diagonalized (lumped) mass matrix was used. The Table 3 shows the dimensionless frequencies computed with the two elements presented here and those reported in the literature. In the table “mode” indicates the number of half-waves in each direction. It can be seen a very good correlation between published and present results.

Furthermore the same plate of the first example, simply supported under sinusoidal load in both directions of the plane, is analyzed by assuming that the load is temporarily applied as a step function (Heaviside). The time integration is performed using Newmark algorithm for the implicit case and central differences within an explicit scheme. For the same discretization used before, with the stiffness matrix in the original configuration and a diagonalized mass matrix, the fundamental periods from a linear eigenvalue analysis are $T_{QL} = 0.1154$ and $T_{TLLL} = 0.1156$. The Fig. 2 shows the vertical displacement of the center of the plate as a function of time. In that figure four curves are included, two correspond to the FSDT (the smaller displacement) and two to ZZRT. The difference in results obtained using implicit and explicit integration schemes are insignificant so only the implicit results are plotted. The differences between the QL and TLLL models are almost null. Note that the vibration amplitude $A_{QL} = 1.348$ and $A_{TLLL} = 1.350$ is slightly below twice the displacement corresponding to the static analysis.

8.4. Spherical sector with line loads

To make comparisons for double curved shells in the non-linear rage the spherical sector shown in Fig. 3 with radius $R = 10$ m and angle $\alpha = 30^o$ is considered. The applied loads are uniform line loads, outward over the meridians A–A ($+x$) and C–C ($-x$) and inward over the meridians B–B ($-y$) and D–D ($+y$).

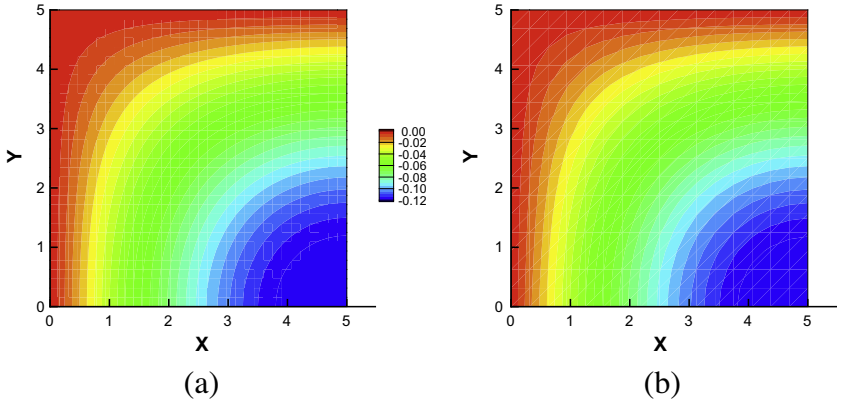

Fig. 1. Amplitude of the additional displacement ψ_x. (a) using QL (b) using TLLL.

Table 3
Natural frequencies of a simple supported plate.

	Ref. [6]		QL		TLLL	
Mode	$a/t = 10$	$a/t = 100$	$a/t = 10$	$a/t = 100$	$a/t = 10$	$a/t = 100$
(1,1)	1.852	11.95	1.851	11.95	1.850	11.92
(1,3)	5.241	36.17	5.324	37.30	5.143	37.02
(3,3)	7.704	49.80	7.679	49.68	7.733	49.48

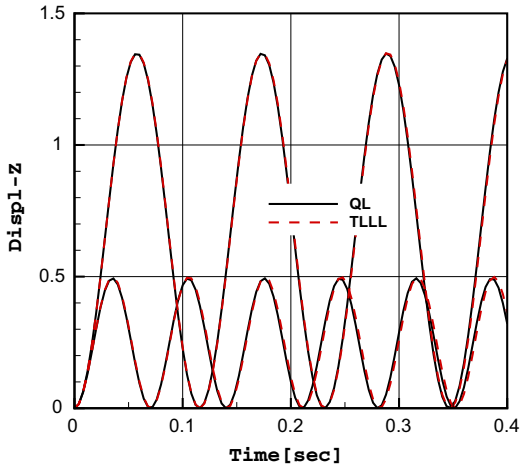

Fig. 2. Simple supported square plate under sinusoidal load. Dynamic analysis.

The sandwich laminate used is number 2 which differs from number 1 in that the core material is much more rigid in the plane of the shell in order to prevent an early collapse. In this case the total thickness is $t = 0.2$ m and the reference line load is $q_0 = 1$ MN/m. Due to symmetry the mesh used covers one quarter of the geometry with 40 divisions in the parallel direction and 14 along the meridian, that leads to a total of 615 nodes and 520 quadrilateral elements or 260 triangular elements. For comparison an eight-node solid element model was used with the same discretization of the middle surface and 6 layers through the thickness. This solid element includes an ANS approach for the transverse shear strains[3] so it can used to model shells with high aspect ratio (in-plane/thickness lengths).

A non-linear geometrical and linear material analysis is performed. The maximum inward displacement is 3 m (30% of the radius). The Fig. 4 plots the inward and outward displacements

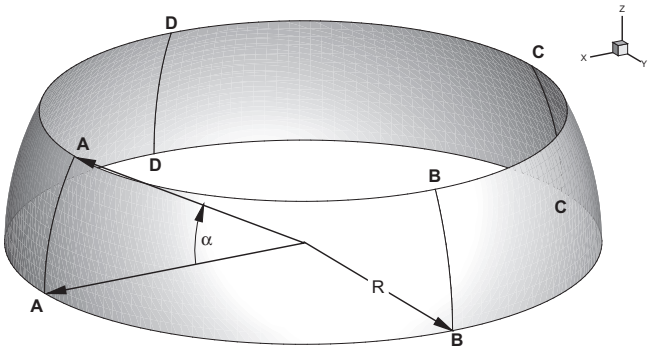

Fig. 3. Spherical sector with line loads.

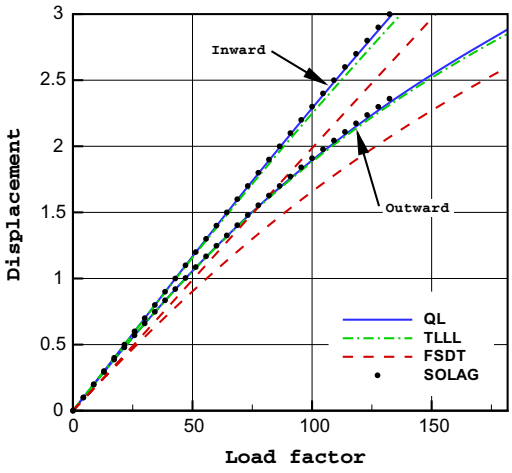

Fig. 4. Spherical sector with line loads. Displacements of the loaded meridians.

of the two points on the lower free side at the loaded meridians. The results shown include those obtained with the quadrilateral element (QL), the triangle (TLLL) and the solid element model (SOLAG). It can be observed an excellent correlation between the results obtained with solid and shell elements. The triangular element is in this case slightly stiffer because the membrane performance is poorer but note also that the number of degrees involved is lower. Results obtained using the FSDT with standard shear coefficients $k_x = k_y = \frac{5}{6}$ have also been included, that solution is clearly stiffer.

Table 4
Critical loads of a clamped cylinder.

Model	Axial load [MN/m]	External pressure [MPa]
Solids	7.040	0.3888
ZZRT	7.093	0.3988
FSDT	20.529	0.6583

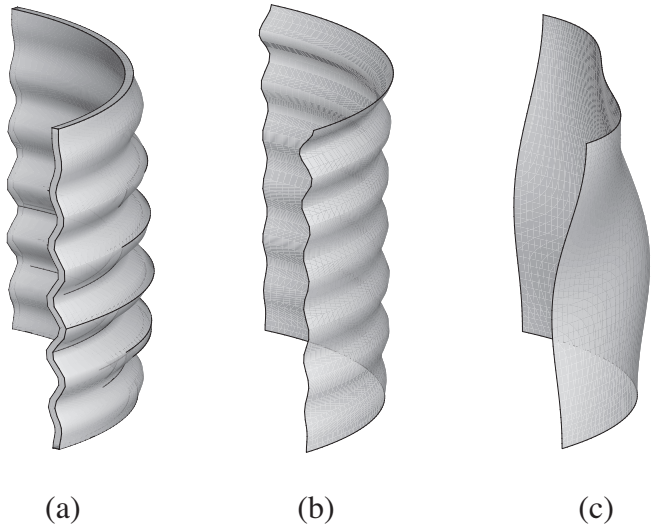

Fig. 5. Buckling mode under axial load (a) solids; (b) ZZRT; (c) FSDT.

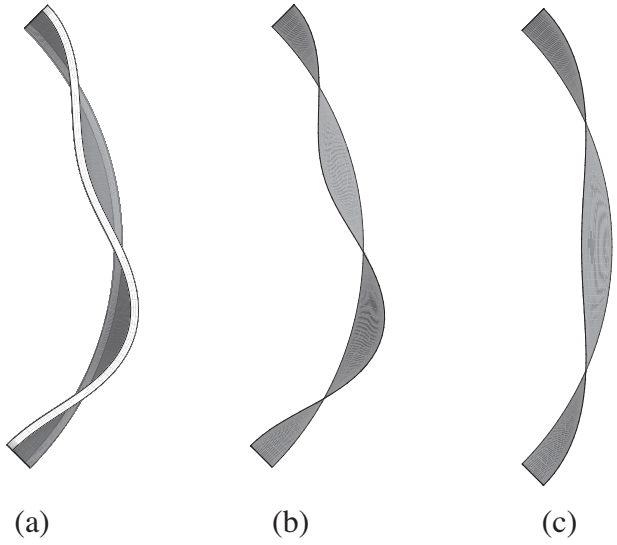

Fig. 6. Buckling mode under external pressure (a) solids; (b) ZZRT; (c) FSDT.

8.5. Buckling of a cylinder

In this example the behavior of a clamped cylinder under alternatively axial and pressure loads is studied. The radius of the cylinder is 10 and the total length 20 while the thickness is $t = 0.25$ with a cross section defined by laminate 2, wherein direction 1 of the laminate is the tangent to the parallel direction. Only one eighth of the cylinder has been meshed (1 quadrant and half the length) setting symmetry conditions on 3 of its edges while the remaining edge is clamped. This boundary conditions arbitrary restricts bifurcation modes to such symmetries but substantially alleviates the numerical solid element model used for comparison. The structured mesh used has 60 divisions along one quadrant and 42 divisions along half cylinder, that leads to 2623 nodes and 2520 `QL` elements. Again a model with 8-node solid elements was considered for comparison. The mesh in this case includes the same discretization used with shell elements for the middle surface and 7 elements in thickness.

The critical loads obtained are indicated in Table 4, a very good correlation is obtained between the solid model and the shell model when the ZZRT is used.

These similarities and differences between critical loads have their correlation with the shape of the buckling modes. In Fig. 5 the buckling modes for axial load are shown. Here it may be noted that in the axial case the buckling mode predicted by FSDT is substantially different from that predicted by the model with 3D elements, while although ZZRT do not show the same number of waves (which may be due to insufficient discretization of the solid model), the pattern is similar. Finally in Fig. 6 buckling modes due to lateral pressure are shown, where the similarity between the results of solid and ZZRT models can again be seen, while the greater rigidity introduced by the FSDT with a lower number of circumferential waves can be appreciated.

9. Conclusions

A possible implementation of the refined zigzag theory (ZZRT) in two finite elements based on the geometrical exact shell theory proposed by Simo et al. has been presented. The elements are a bilinear quadrilateral and a six-node triangle with a linear interpolation of the middle surface geometry and a linear (non-conforming) interpolation of the director field.

The main issues in the implementation are:

- The hierarchical additional displacements are defined as the in-plane local components in a convective system of the middle surface of the shell.
- It is restricted to small elastic strains then no distinction is made between different strain measures.
- The strain tensor components are computed as the sum of those arising from the configuration change of the middle surface geometry and its director field (FSDT) plus those resulting from the additional displacements as derived by the ZZRT.
- The same assumed natural strain approach (ANS) used for transverse shear in the FSDT is also applied to the additional strains from the ZZRT transverse shear.
- A diagonalized (lumped) mass matrix has been considered for dynamical problems.

The main conclusions that may be mentioned are:

- Both proposed elements behave well and converge to the ZZRT results in the plates examples considered, both in static equilibrium and natural vibration frequencies.
- Use of a diagonalized mass matrix shows and adequate dynamic behavior with identical results in both time integration schemes (implicit and explicit) considered.
- The comparison with solid element models in double curved shell examples shows a very good agreement which validates not only the elements but also increases the predictive potential of the ZZRT.
- The evaluation of critical loads on curved geometries shows an excellent correlation when compared with solid models and indicates again the limitation of the FSDT.
- The assumed natural strain (ANS) approach for transverse shear works correctly. The same can be said of the stabilization scheme used for the transverse shear in the `TLLL` element with one integration point.

Acknowledgments

Financial support from CONICET and SeCyT-UNC is gratefully acknowledged. The author also acknowledges Prof. Eugenio Oñate (CIMNE-UPC) for having introduced him in the subject.

References

[1] Carrera E. Historical review of zig-zag theories for multilayered plates and shells. Appl Mech Rev 2003;56:298–308.
[2] Eijo A, Oñate E, Oller S. A four-noded quadrilateral element for composite laminated plates/shells using the refined zigzag theory. Int J Numer Meth Eng 2013;95:631–60.
[3] Flores FG, Oñate E. Un elemento de sólido con una mejora en el comportamiento del corte transversal para el tratamiento de láminas. Rev. Int. Métodos Numér. Cál. Diseño Ing. 2011;27(4):256–68.
[4] Flores FG, Oñate E, Zárate F. New assumed strain triangles for non linear shell analysis. Comput Mech 1995;17:107–14.
[5] Gherlone M, Tessler A, Di Sciuva M. C^0 beam element based on the refined zigzag theory for multilayered composite and sandwich laminates. Compos Struct 2011;93:2882–94.
[6] Iurlaro L, Gherlone M, Di Sciuva M, Tessler. Assessment of the refined zigzag theory for bending, vibration, and buckling of sandwich plates: a comparative study of different theories. Compos Struct 2013;106:777–92.
[7] Kirchhoff G. Über das gleichgewicht und die bewegung einer elastischen scheibe. Journal fnr die reine und Angewandte Mathematik 1850;40:51–88.
[8] Martinez X, Rastellini F, Oller S, Flores FG, Oñate E. Computationally optimized formulation for the simulation of composite materials and delamination failures. J Compos Part B 2011;42:134–44.
[9] Oñate E, Eijo A, Oller S. Simple and accurate two-noded beam element for composite laminated beams using a refined zigzag theory. Comput Meth Appl Mech Eng 2012;213–216:362–82.
[10] Reddy JN. Mechanics of laminated composite plates and shells: theory and analysis. CRC Press; 2004.
[11] Reddy JN, Robbins DH. Theories and computational models for composite laminates. Appl Mech Rev 1994;47:147–65.
[12] Reissner E. The effect of transverse shear deformation on the bending of elastic plates. J Appl Mech 1945;12:69–79.
[13] Simo JC, Fox DD. On a stress resultant geometrically exact shell model. Part i: formulation and optimal parametrization. Comput Meth Appl Mech Eng 1989;72:267–304.
[14] Simo JC, Fox DD, Rifai MS. On a stress resultant geometrically exact shell model. Part iii: computational aspects of the non-linear theory. Comput Meth Appl Mech Eng 1990;79:21–70.
[15] Tessler A, Di Sciuva M, Gherlone M. A consistent refinement of first-order shear deformation theory for laminated composite and sandwich plates using improved zigzag kinematics. J Mech Mater Struct 2010;5:341–67.